Dyskeratosis Congenita and Cancer in Mice Deficient in Ribosomal RNA Modification

Davide Ruggero, *et al.*

Science **299**, 259 (2003);
DOI: 10.1126/science.1079447

transcriptional cofactors such as PIAS or other, unknown factors.

Our discovery of *DJ-1* mutations in PARK7 opens new avenues for understanding the neuronal function of DJ-1, that, when lost, causes neurodegeneration. Furthermore, the observation that DJ-1 may be involved in the oxidative stress response links a genetic defect in this pathway to the development of parkinsonism, with possible implications for understanding the pathogenesis of the common forms of PD.

References and Notes

1. A. E. Lang, A. M. Lozano, *N. Engl. J. Med.* **339**, 1044 (1998).
2. M. M. Mouradian, *Neurology* **58**, 179 (2002).
3. C. M. van Duijn *et al.*, *Am. J. Hum. Genet.* **69**, 629 (2001).
4. V. Bonifati *et al.*, *Ann. Neurol.* **51**, 253 (2002).
5. www.ncbi.nlm.nih.gov
6. Materials and methods are available as supporting material on *Science* Online.
7. E. M. Valente et al., *Am. J. Hum. Genet.* **68**, 895 (2001).
8. G. Vriend, *J. Mol. Graph* **8**, 52 (1990).
9. E. Krieger, G. Koraimann, G. Vriend, *Proteins* **47**, 393 (2002).
10. X. Du *et al.*, *Proc. Natl. Acad. Sci. U.S.A.* **97**, 14079 (2000).
11. B. Rost, *Protein Eng.* **12**, 85 (1999).
12. M. K. Kim, Y. K. Kang, *Protein Sci.* **8**, 1492 (1999).
13. D. Nagakubo *et al.*, *Biochem. Biophys. Res. Commun.* **231**, 509 (1997).
14. Y. Hod, S. N. Pentyala, T. C. Whyard, M. R. El-Maghrabi, *J. Cell Biochem.* **72**, 435 (1999).
15. K. Takahashi *et al.*, *J. Biol. Chem.* **276**, 37556 (2001).
16. N. Kotaja, U. Karvonen, O. A. Janne, J. J. Palvimo, *Mol. Cell. Biol.* **22**, 5222 (2002).
17. A. Mitsumoto *et al.*, *Free Radic. Res.* **35**, 301 (2001).
18. A. Mitsumoto, Y. Nakagawa, *Free Radic. Res.* **35**, 885 (2001).
19. H. de Nobel *et al.*, *Yeast* **18**, 1413 (2001).
20. B. I. Giasson, H. Ischiropoulos, V. M.-Y. Lee, J. Q. Trojanowski, *Free Radic. Biol. Med.* **32**, 1264 (2002).
21. M. Hashimoto *et al.*, *J. Biol. Chem.* **277**, 11465 (2002).
22. D.-H. Hyun *et al.*, *J. Biol. Chem.* **277**, 28572 (2002).

23. We thank the members of the families examined for their participation; P. Chiurazzi, E. Fabrizio, R. J. Galjaard, T. Gasser, M. Horstink, S. Rossetti, L. A. Severijnen, P. J. Snijders, and C. Wijmenga for their contributions; T. deVries-Lentsch for artwork. This work was funded in part by the Parkinson Disease Foundation/National Parkinson Foundation (USA), the Princess Beatrix Foundation (Netherlands), the Stichting Klinische Genetica Rotterdam, the Netherlands Organization for Scientific Research (NWO), and the Ministero dell'Istruzione, Università e Ricerca (MIUR, Italy).

Supporting Online Material

www.sciencemag.org/cgi/content/full/1077209/DC1
Materials and Methods
SOM Text
Figs. S1 to S3
References and Notes

9 August 2002; accepted 11 November 2002
Published online 21 November 2002;
10.1126/science.1077209
Include this information when citing this paper.

Dyskeratosis Congenita and Cancer in Mice Deficient in Ribosomal RNA Modification

Davide Ruggero,[1,2] Silvia Grisendi,[1,2] Francesco Piazza,[1,2] Eduardo Rego,[1,2,3] Francesca Mari,[1,2] Pulivarthi H. Rao,[4] Carlos Cordon-Cardo,[2] Pier Paolo Pandolfi[1,2]*

Mutations in *DKC1* cause dyskeratosis congenita (DC), a disease characterized by premature aging and increased tumor susceptibility. The *DKC1* protein binds to the box H + ACA small nucleolar RNAs and the RNA component of telomerase. Here we show that hypomorphic *Dkc1* mutant (*Dkc1^m*) mice recapitulate in the first and second generations (G1 and G2) the clinical features of DC. *Dkc1^m* cells from G1 and G2 mice were impaired in ribosomal RNA pseudouridylation before the onset of disease. Reductions of telomere length in *Dkc1^m* mice became evident only in later generations. These results suggest that deregulated ribosome function is important in the initiation of DC, whereas telomere shortening may modify and/or exacerbate DC.

Dyskeratosis congenita (DC) is a rare X-linked recessive disease caused by point mutations in the *DKC1* gene (*1*). Individuals with DC display features of premature aging, as well as nail dystrophy, mucosal leukoplakia, interstitial fibrosis of the lung, and increased susceptibility to cancer (*2*, *3*). The tissues consistently affected by DC, such as the bone marrow and skin, are characterized by a high turnover of their progenitor cells.

DKC1 codes for dyskerin, a putative pseudouridine synthase, which is in a complex with box H + ACA small nuclear RNAs and mediates posttranscriptional modification of ribosomal RNA (rRNA) through conversion of uridine (U) to pseudouridine (Ψ) (*4*–*6*). Point mutations in the yeast homolog of *DKC1* and loss of *DKC1* expression in *Dro-*

[1]Molecular Biology Program, [2]Department of Pathology, Memorial Sloan-Kettering Cancer Center, Sloan-Kettering Institute, 1275 York Avenue, New York, NY 10021, USA. [3]Center for Cell-Based Therapy, FUNDHERP, University of São Paulo, Ribeirão Preto, SP 14049-900 Brazil. [4]Department of Pediatrics, Baylor College of Medicine, Houston, TX 77030, USA.

*To whom correspondence should be addressed. E-mail: p-pandolfi@ski.mskcc.org

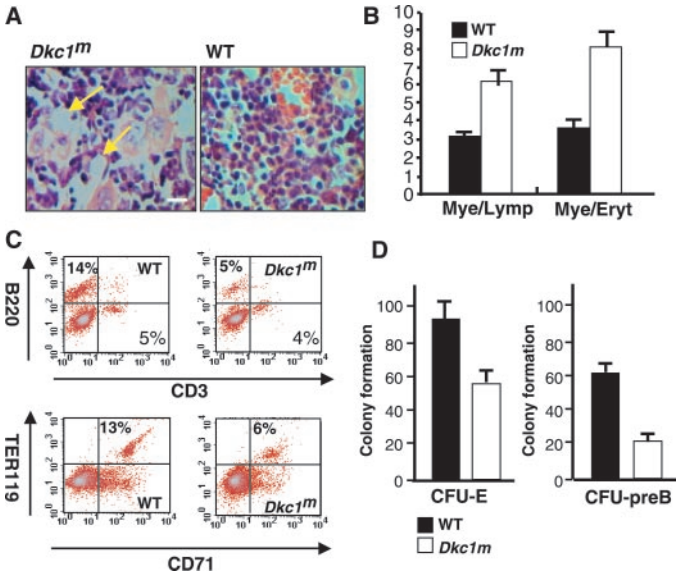

Fig. 1. Bone marrow (BM) failure in *Dkc1^m* mice. (**A**) BM sections stained with hematoxylin and eosin, showing decreased BM cellularity in *Dkc1^m* mice, as compared with WT controls. Arrows indicate adipose tissue. Scale bar, 50 μm. (**B**) Cytomorphological analysis of *Dkc1^m* and WT BM cytospin preparations. Bars represent the myeloid-to-lymphoid (left) and the myeloid-to-erythroid ratios (right) of BM cells. Each bar represents the mean ± SE (error bars) from 14 mice. (**C**) Flow cytometric analysis of *Dkc1^m* BM. The dot plot cytograms show the decrease in B lym phocytes (CD3 and B220 positive cells, top row, top left quadrant) and erythroid cells (CD71 and TER119 double-positive cells, bottom row, top right quadrant) in *Dkc1^m* BM. (**D**) BM colony-forming assay in WT and *Dkc1^m* mice. BM cultures were scored for the number of erythroid and B lymphocyte colony-forming units (CFU-E and CFU-preB, respectively), and the data are expressed as the percentage of colony numbers present in the cultures. Each value represents the mean ± SE (error bars) from triplicates of one of three independent experiments performed on healthy *Dkc1^m* mice before the onset of disease.

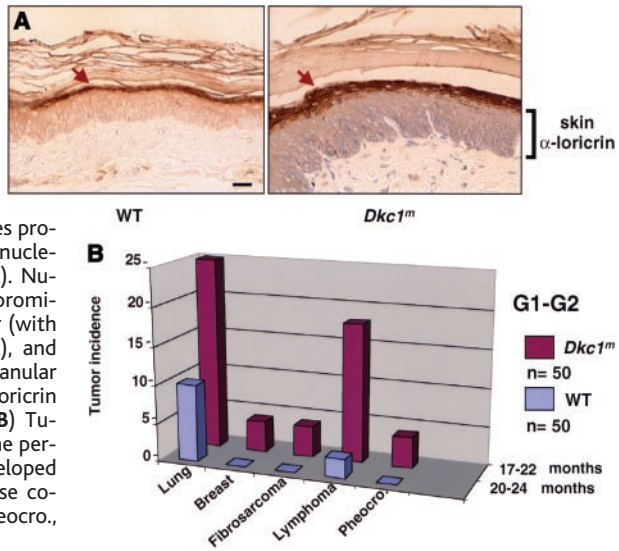

Fig. 2. Dyskeratosis of the skin and increased tumor susceptibility in *Dkc1*^{m} mice. (**A**) Histopathological analysis of *Dkc1*^{m} skin. Photomicrographs of skin from the palm of a WT mouse and a *Dkc1*^{m} mouse. The epidermis of 7 out of 25 *Dkc1*^{m} mice analyzed shows hyperplastic changes produced by an expansion of the nucleated cell layers (square bracket). Nucleoli of keratinocytes can be prominently seen in the spinous layer (with the area noted by the bracket), and there is an increase in the granular layer stained with antibody to loricrin (arrows). Scale bar, 200 μm. (**B**) Tumor incidence is expressed as the percentage of mice that developed tumors in WT and *Dkc1*^{m} mouse cohorts over time (n = 50). Pheocro., pheocromocytoma.

sophila reduce pseudouridylation and processing of rRNA (*7*–*10*). Mutations in the catalytic domain of dyskerin required for rRNA pseudouridylation have been implicated in Hoyeraal-Hreidarsson syndrome, which is characterized by a more severe spectrum of pathologies than that of DC, including immunodeficiency, growth retardation, and microcephaly (*11*, *12*).

Dyskerin is also physically associated with the RNA component of human telomerase (hTR), which contains a H + ACA RNA motif (*13*). Cell lines derived from individuals with DC have reduced telomerase activity and shorter telomeres, as compared with those from individuals without DC (*13*). Primary cells from the peripheral blood of individuals with DC also have shorter telomeres than those of individuals without DC, but they have normal levels of

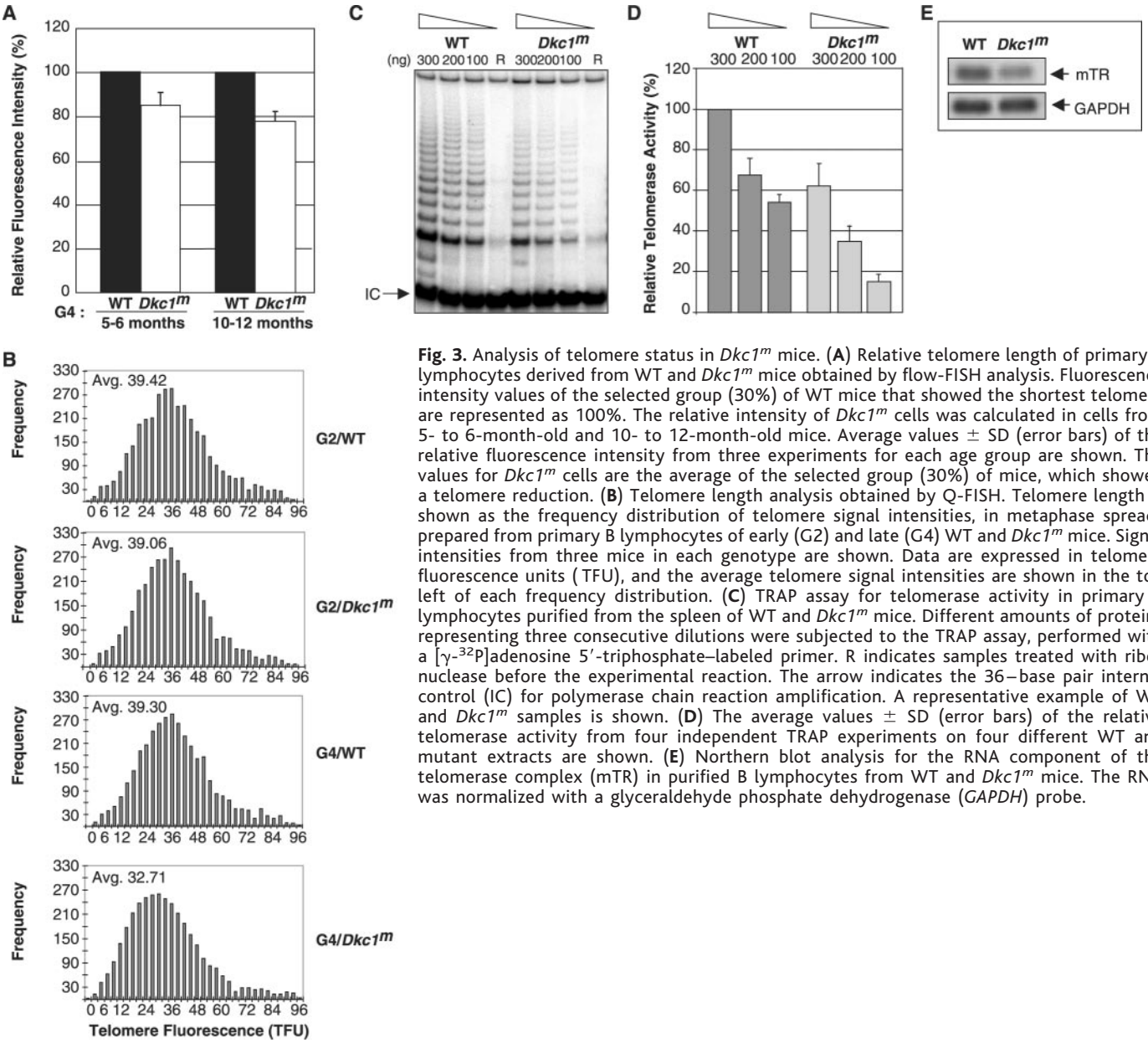

Fig. 3. Analysis of telomere status in *Dkc1*^{m} mice. (**A**) Relative telomere length of primary B lymphocytes derived from WT and *Dkc1*^{m} mice obtained by flow-FISH analysis. Fluorescence intensity values of the selected group (30%) of WT mice that showed the shortest telomere are represented as 100%. The relative intensity of *Dkc1*^{m} cells was calculated in cells from 5- to 6-month-old and 10- to 12-month-old mice. Average values ± SD (error bars) of the relative fluorescence intensity from three experiments for each age group are shown. The values for *Dkc1*^{m} cells are the average of the selected group (30%) of mice, which showed a telomere reduction. (**B**) Telomere length analysis obtained by Q-FISH. Telomere length is shown as the frequency distribution of telomere signal intensities, in metaphase spreads prepared from primary B lymphocytes of early (G2) and late (G4) WT and *Dkc1*^{m} mice. Signal intensities from three mice in each genotype are shown. Data are expressed in telomere fluorescence units (TFU), and the average telomere signal intensities are shown in the top left of each frequency distribution. (**C**) TRAP assay for telomerase activity in primary B lymphocytes purified from the spleen of WT and *Dkc1*^{m} mice. Different amounts of proteins representing three consecutive dilutions were subjected to the TRAP assay, performed with a [γ-^{32}P]adenosine 5′-triphosphate–labeled primer. R indicates samples treated with ribonuclease before the experimental reaction. The arrow indicates the 36–base pair internal control (IC) for polymerase chain reaction amplification. A representative example of WT and *Dkc1*^{m} samples is shown. (**D**) The average values ± SD (error bars) of the relative telomerase activity from four independent TRAP experiments on four different WT and mutant extracts are shown. (**E**) Northern blot analysis for the RNA component of the telomerase complex (mTR) in purified B lymphocytes from WT and *Dkc1*^{m} mice. The RNA was normalized with a glyceraldehyde phosphate dehydrogenase (*GAPDH*) probe.

telomerase activity (*14*). hTR is mutated in an autosomal dominant form of DC, which has a phenotype that is similar to, but markedly milder than, that of X-linked DC (*15*). Therefore, an outstanding question is whether the disease state associated with mutations in *DKC1* is the result of a defect in rRNA modification, telomere maintenance, or both. The mouse is an ideal model organism to address this issue genetically because defects in telomerase function resulting in telomere attrition would only be manifest in late generations (*16*, *17*).

To investigate the role of *DKC1* in disease pathogenesis, we generated hypomorphic *Dkc1* mutant mice (*Dkc1^m*) (Fig. S1, A and B and supporting online text) (*18*). *Dkc1^m* mice were born at normal Mendelian ratios with no overt developmental defects. Cells from hemizygous male and heterozygous female *Dkc1^m* mice displayed a decreased level of *Dkc1* expression (four- and twofold, respectively) (Fig. S1C).

One of the most consistent features of human DC is bone marrow failure (BMF). Starting from 6 months of age, ~60% of *Dkc1^m* mice in the first and second generations (G1 and G2, respectively) presented with severe anemia [mean hemoglobin at 8 months was 10.6 ± 4 g/dl, versus 15.1 ± 1.7 g/dl in wild-type (WT) controls ($P < 0.001$, $n = 16$ in each group)] and lymphopenia [mean absolute number of lymphocytes was 2428 ± 1978 per μl, versus 5352 ± 2945 per μl in WT controls ($P = 0.01$)]. Because of the lymphopenia, the *Dkc1^m* mice became mildly leukopenic [mean white blood cell count was 4526 ± 3311 per μl, versus 8215 ± 3795 per μl in WT controls ($P = 0.07$)]. Some of the *Dkc1^m* mice also had reduced platelet counts, as well as a specific decrease in B lymphocytes (*19*). Analysis of bone marrow (BM) from anemic *Dkc1^m* mice revealed a decrease in cellularity, with a relative increase in fat and fibrous tissue (Fig. 1A) [mean BM cellularity at 8 months was 67.8 ± 7.1%, versus 87.3 ± 5.7% in WT controls ($P < 0.0001$, $n = 14$ per group)]. A decrease in erythroid and lymphoid cells (Fig. 1B) and, in certain cases, a decrease in myeloid cells (*19*) were observed in BM cytospins from *Dkc1^m* mice. Flow cytometric analysis confirmed the reduction in erythroid cells and B lymphocytes (Fig. 1C).

We next performed BM colony-forming assays to assess the clonogenic and differentiation potential of hematopoietic precursors from WT and *Dkc1^m* mice before the onset of disease. The *Dkc1^m* mice exhibited a reduced number of erythroid and B colony-forming units (Fig. 1D). [^{3}H]thymidine incorporation assays in BM liquid cultures revealed no difference in the proliferation rate of *Dkc1^m* and WT cells (*19*). Most analyzed mice were G2 hemizygous males. However, features of BMF were also observed at a lower penetrance in heterozygous G1 and G2 female *Dkc1^m* mice (*19*), consistent with the observation that some human female carriers of *DKC1* mutations display features of X-linked DC (*20*, *21*). Thus, BMF (one of the distinctive features of DC) is highly penetrant in G1 and G2 *Dkc1^m* mice.

Dkc1^m mice starting from the G1 generation showed additional pathological features, including dyskeratosis of the skin (Figs. 2A and S3, A and B), extramedullary hematopoieis associated with splenomegaly (Fig. S2), and abnormalities in the lungs and kidneys (Fig. S3, C through F). A subset of individuals with DC develop malignant tumors of various histological origin (*2*). *Dkc1^m* mice were highly prone to tumors and developed a variety of them (Fig. 2B), the most common being lung and mammary gland tumors, as well as one case of renal cell carcinoma (Figs. 2B and S4, A through F) (*19*). Strikingly, 50% of *Dkc1^m* mice developed tumors during their life-span, suggesting that *Dkc1* is an important tumor-suppressor gene in vivo. All of the defects observed in the *Dkc1^m* mice have been previously documented in human DC (*2*, *3*). Thus, the hypomorphic *Dkc1^m* mouse is a faithful model of the human disease.

To determine the molecular basis for DC in the *Dkc1^m* mice, we examined their telomere status. As assessed by flow–fluorescence in situ hybridization (flow-FISH), a reduction in telomere length was first evident in 30% of early fourth generation (G4) *Dkc1^m* mice, as compared to WT mice ($n = 20$ in each group) (Fig. 3A). There were no detectable changes in telomere length in *Dkc1^m* mice before G4 (Fig. S5A). Furthermore, using quantitative-FISH (Q-FISH) analysis (*22*) to quantitate the relative number of telomere repeats on individual chromosome ends, we did not detect any differences between early generation *Dkc1^m* mice and WT mice, whereas G4 *Dkc1^m* mice showed a loss of telomere repeats, which is consistent with the flow-FISH data (Fig. 3B).

We next investigated whether the decreased telomere length in early G4 mice was accompanied by a decrease in telomerase activity. A telomeric repeat amplification protocol (TRAP) assay revealed a 40% decrease in telomerase activity in *Dkc1^m* cells, as compared with WT controls, and this was associated with a 1.2-fold reduction in mouse telomerase RNA (mTR) levels (Fig. 3, C through E). These data indicate that although dyskerin may be an integral component of the telomerase complex, the DC phe-

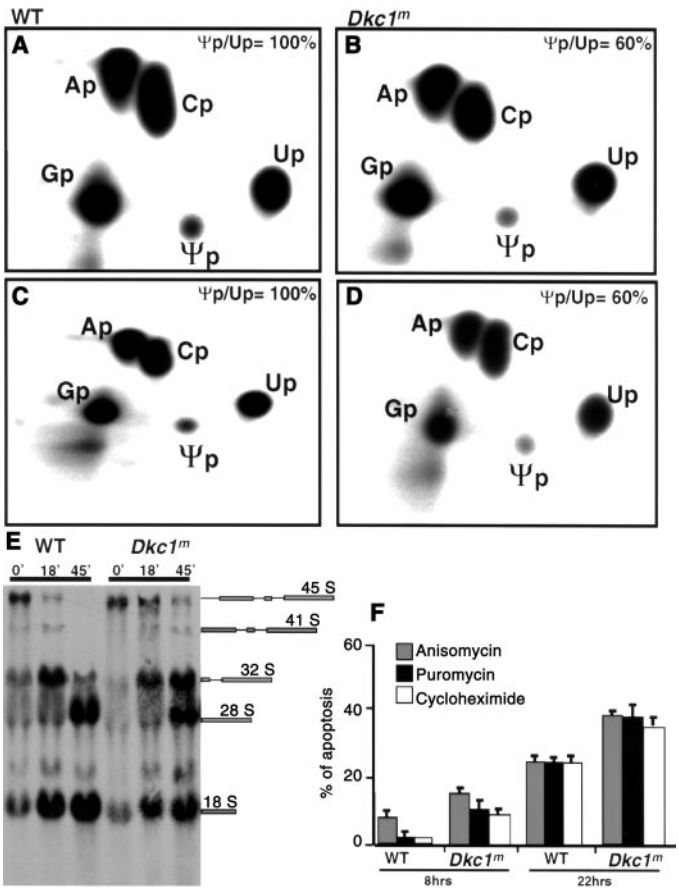

Fig. 4. Impaired rRNA pseudouridylation and ribosome function in *Dkc1^m* mice. (**A** through **D**) Ψ formation in rRNA from G2 WT and *Dkc1^m* mutant B lymphocytes. Representative TLC analysis of labeled 28*S* (A) and 18*S* rRNA (C) from WT cells. There is a decrease in Ψp formation relative to Up in both 28*S* (B) and 18*S* rRNA (D) from *Dkc1^m* cells. Ψp/Up from *Dkc1^m* was then normalized against that for the WT, adjusted to 100%. The averages for 100% of the animals studied ($n = 8$) are [Ψp/Up 28*S*: WT, 100%; *Dkc1^m*, 78 ± 9.3 ($P < 0.05$)] [Ψp/Up 18*S*: WT, 100%; *Dkc1^m*, 76 ± 10 ($P < 0.05$)]. Spots corresponding to Ap (adenosine 3′-monophosphate), Cp (eytidine 3′-monophosphate), Gp (guanosine 3′-monophosphate), Up, and Ψp are indicated. (**E**) Pulse-chase labeling experiments of rRNA from G2 WT and *Dkc1^m* B lymphocytes. There is an accumulation of 45*S*, 41*S*, and 32*S* rRNA species with a concomitant decrease in the mature 18*S* and 28*S* rRNA from *Dkc1^m* cells. A schematic representation of all intermediate and mature rRNA species is illustrated. (**F**) G2 *Dkc1^m* and WT mouse embryonic fibroblasts (MEFs) were treated with anisomycin (20 μg/ml), cyclohexamide (20 μg/ml), and puromycin (40 μg/ml). Apoptosis was measured by subdiploid peak fluorescence-activated cell sorting analysis. The average of three independent experiments ± SD (error bars) from early passage MEFs is shown. Cells of the same passage from *Dkc1^m* and WT mice were studied.

notype in the early generation *Dkc1*^{m} mice is likely to be independent of its role in maintaining telomere length.

We next examined rRNA pseudouridylation in early generation *Dkc1*^{m} mice. The nucleotide composition of 28*S* and 18*S* rRNA was analyzed with two-dimensional thin-layer chromatography (TLC), and the ratio of modified (pseudouridine 3′-monophosphate) to unmodified uridines (uridine 3′-monophosphate) (Ψp/Up) was calculated. In six out of eight *Dkc1*^{m} samples analyzed, there was a 10 to 40% reduction in Ψp/Up for both the 28*S* and 18*S* rRNAs (Fig. 4, A through D). Analysis of newly synthesized rRNA revealed that *Dkc1*^{m} cells contained immature intermediates of 45*S*, 41*S*, and 32*S* rRNA at time points at which these rRNA species in WT controls were fully processed (Fig. 4E). Finally, to assess ribosome function, we measured the sensitivity of WT and *Dkc1*^{m} cells to drugs that inhibit translation (*23*, *24*). *Dkc1*^{m} cells were hypersensitive to these drugs, undergoing apoptosis at a markedly higher rate than WT cells (Fig. 4F). These results indicate that dyskerin acts as a pseudouridine synthase in mammalian cells and that impairment of its activity disrupts ribosome function.

Dkc1^{m} mice recapitulate the major features of DC, including an increased susceptibility to tumor formation. G1 and G2 *Dkc1*^{m} mice presented with DC and showed alterations in rRNA modification, whereas defects in telomere length were not evident until G4 mice. This is in agreement with the analysis of mTR knockout mice, which show an aging phenotype and tumor susceptibility only in late generations (fourth through sixth) (*16*). The fact that *Dkc1*^{m} mice develop the full spectrum of DC features in G1 and G2 strongly suggests that deregulated ribosome function is important for the initiation of DC and that impairment in telomerase activity in *Dkc1*^{m} mice may modify and/or exacerbate the disease in later generations. Although we cannot exclude additional unrecognized functions of dyskerin, our results establish a role for deregulated rRNA modification in tumor formation and disease pathogenesis.

References and Notes

1. N. S. Heiss *et al.*, *Nature Genet.* **19**, 32 (1998).
2. I. Dokal, *Br. J. Haematol.* **110**, 768 (2000).
3. S. W. Knight *et al.*, *Hum. Genet.* **108**, 299 (2001).
4. J. Ni, A. L. Tien, M. J. Fournier, *Cell* **89**, 565 (1997).
5. Y. Yang *et al.*, *Mol. Biol. Cell* **11**, 567 (2000).
6. W. A. Decatur, M. J. Fournier, *Trends Biochem. Sci.* **27**, 344 (2002).
7. D. L. Lafontaine, C. Bousquet-Antonelli, Y. Henry, M. Caizergues-Ferrer, D. Tollervey, *Genes Dev.* **12**, 527 (1998).
8. Y. Zebarjadian, T. King, M. J. Fournier, L. Clarke, J. Carbon, *Mol. Cell. Biol.* **19**, 7461 (1999).
9. B. Phillips *et al.*, *Mol. Gen. Genet.* **260**, 20 (1998).
10. E. Giordano, I. Peluso, S. Senger, M. Furia, *J. Cell Biol.* **144**, 1123 (1999).
11. S. W. Knight *et al.*, *Br. J. Haematol.* **107**, 335 (1999).
12. R. Yaghmai *et al.*, *J. Pediatr.* **136**, 390 (2000).
13. J. R. Mitchell, E. Wood, K. Collins, *Nature* **402**, 551 (1999).
14. T. J. Vulliamy, S. W. Knight, P. J. Mason, I. Dokal, *Blood Cells Mol. Dis.* **27**, 353 (2001).
15. T. Vulliamy *et al.*, *Nature* **413**, 432 (2001).
16. K. L. Rudolph *et al.*, *Cell* **96**, 701 (1999).
17. H. W. Lee *et al.*, *Nature* **392**, 569 (1998).
18. Materials and methods are available as supporting material on *Science* Online.
19. D. Ruggero *et al.*, data not shown.
20. S. W. Knight *et al.*, *Br. J. Haematol.* **103**, 990 (1998).
21. K. Devriendt *et al.*, *Am. J. Hum. Genet.* **60**, 581 (1997).
22. P. M. Lansdorp *et al.*, *Hum. Mol. Genet.* **5**, 685 (1996).
23. M. Masurekar, E. Palmer, B. I. Ono, J. M. Wilhelm, F. Sherman, *J. Mol. Biol.* **147**, 381 (1981).
24. R. J. Nelson, T. Ziegelhoffer, C. Nicolet, M. Werner-Washburne, E. A. Craig, *Cell* **71**, 97 (1992).

25. We thank M. Barna for helpful discussion and critical reading of the manuscript; A. Di Cristofano, M. S. Jiao, and W. Xu for assistance with several experiments; P. Lansdorp and E. Chavez for critical advice and reagents; K. Manova and M. Leversha for assistance with microscopy; and P. Salomoni and L. Luzzatto for helpful discussion. S. G. is supported by the American Italian Cancer Foundation. P.P.P. is a Scholar of the Leukemia and Lymphoma Society.

Supporting Online Material

www.sciencemag.org/cgi/content/full/299/5604/259/DC1
Materials and Methods
SOM Text
Figs. S1 to S4
References

16 October 2002; accepted 7 November 2002

Role of a Highly Conserved Bacterial Protein in Outer Membrane Protein Assembly

Romé Voulhoux, Martine P. Bos, Jeroen Geurtsen, Maarten Mols, Jan Tommassen*

After transport across the cytoplasmic membrane, bacterial outer membrane proteins are assembled into the outer membrane. Meningococcal Omp85 is a highly conserved protein in Gram-negative bacteria, and its homolog Toc75 is a component of the chloroplast protein-import machinery. Omp85 appeared to be essential for viability, and unassembled forms of various outer membrane proteins accumulated upon Omp85 depletion. Immunofluorescence microscopy revealed decreased surface exposure of outer membrane proteins, which was particularly apparent at the cell-division planes. Thus, Omp85 is likely to play a role in outer membrane protein assembly.

The cell envelope of Gram-negative bacteria consists of an outer membrane (OM) and an inner membrane (IM), separated by the periplasm. The IM is a phospholipid bilayer, whereas the OM is asymmetric with phospholipids and lipopolysaccharides (LPS) in the inner and outer leaflet, respectively. Whereas integral IM proteins are mostly α-helical, OM proteins (OMPs) present a different structure, the β barrel (*1*). OMPs are synthesized in the cytoplasm with an NH_2-terminal signal sequence required for IM translocation by the Sec machinery (*2*). After translocation, the signal sequence is cleaved off, releasing the mature protein in the periplasm. Little is known about the subsequent steps in OMP biogenesis. OMPs fold in the periplasm before their insertion into the OM (*3*), and LPS stimulates the folding of OMPs in vitro (*4*). Also, the periplasmic chaperone SurA stimulates OMP folding (*5*), whereas another periplasmic protein, Skp, plays an unidentified role in OMP biogenesis (*6*). The insertion of proteins into membranes generally requires a proteinaceous machinery. However, no components of the putative OMP insertion machinery have been identified. Such components are likely to be conserved among Gram-negative bacteria and essential for their viability. A protein possibly fulfilling these criteria is the surface antigen designated Omp85 in *Neisseria* spp. and D15 in *Haemophilus* spp. Genes encoding Omp85/D15 homologs are present in all Gram-negative bacteria examined (*7*) [fig. S2 (*8*)]. Attempts to delete the structural gene for this protein in *Haemophilus ducreyi* and *Synechocystis* sp. were unsuccessful, suggesting it is an essential protein (*7, 9*). Furthermore, because the *omp85* gene is located in close proximity to other genes involved in the biogenesis of OM components (*8*), we investigated the possible function of the neisserial Omp85 in OMP assembly.

To verify whether Omp85 was essential for viability, we inactivated the chromosomal *omp85* gene in a strain carrying an intact *omp85* gene under an isopropyl-β-D-thiogalactopyranoside (IPTG)–inducible promoter on a plasmid, designated pRV2100 [fig. S1 (*8*)]. Wild-type and *omp85*-mutant bacteria, both containing pRV2100, were grown on a plate containing 0.1 mM IPTG and then streaked onto plates containing IPTG or glucose (Fig. 1A). The wild-type strain grew normally overnight on all plates, whereas the mutant strain failed to form

Department of Molecular Microbiology and Institute of Biomembranes, Utrecht University, 3584 CH Utrecht, Netherlands.

*To whom correspondence should be addressed. E-mail: j.p.m.tommassen@bio.uu.nl